JVSTB
JOURNAL OF VACUUM SCIENCE AND TECHNOLOGY B

# Understanding the relationship between true and measured resist feature critical dimension and line edge roughness using a detailed scanning electron microscopy simulator

Richard A. Lawson and Clifford L. Henderson

Citation: J. Vac. Sci. Technol. B **28**, C6H34 (2010); doi: 10.1116/1.3517717
View online: http://dx.doi.org/10.1116/1.3517717
View Table of Contents: http://avspublications.org/resource/1/JVTBD9/v28/i6
Published by the AVS: Science & Technology of Materials, Interfaces, and Processing

## Additional information on J. Vac. Sci. Technol. B

Journal Homepage: http://avspublications.org/jvstb
Journal Information: http://avspublications.org/jvstb/about/about_the_journal
Top downloads: http://avspublications.org/jvstb/top_20_most_downloaded
Information for Authors: http://avspublications.org/jvstb/authors/information_for_contributors

ADVERTISEMENT


Downloaded 22 Apr 2013 to 130.207.50.120. Redistribution subject to AVS license or copyright; see http://avspublications.org/jvstb/about/rights_and_permissions

# Understanding the relationship between true and measured resist feature critical dimension and line edge roughness using a detailed scanning electron microscopy simulator

Richard A. Lawson and Clifford L. Henderson[a)]
*School of Chemical and Biomolecular Engineering, Georgia Institute of Technology, Atlanta, Georgia 30332-0100*

(Received 12 July 2010; accepted 25 October 2010; published 30 November 2010)

Top-down critical dimension scanning electron microscopy (SEM) is still the workhorse metrology tool used for nanoscale structure analysis, such as measurement of photoresist features, during integrated circuit manufacturing. However, the degree to which top-down SEM imaging can accurately be used to quantitatively determine the size, shape, and roughness characteristics of three-dimensional structures such as photoresist features has not been carefully characterized. A rigorous Monte Carlo simulation of scanning electron microscopy has been developed to probe the relationship between the roughness of a three-dimensional feature and the line edge roughness (LER) as measured by SEM. The model uses the differential Mott cross section to compute elastic scattering, while inelastic scattering and secondary electron generation are handled using dielectric function theory. The model can calculate the electron scattering for any arbitrary three-dimensional geometry. Experimental SEM measurements of photoresist nanostructures show good agreement with the simulation output. The critical dimension of the resist determined from SEM best matches the true resist feature width when the line edge is defined using a high image threshold because the roughness on the outer edge of the resist tends to cause an increase in SEM signal that is nonproportional to the amount of material on the outer edge of the feature. LER determined from SEM was found to be significantly smaller than the true resist feature sidewall roughness. The measured LER is typically greater than 50% smaller than the actual sidewall roughness. © *2010 American Vacuum Society.* [DOI: 10.1116/1.3517717]

## I. INTRODUCTION

There is an ever increasing need to accurately measure the size and shape of nanoscale structures in the semiconductor industry. While there are a number of different tools that can provide information at this length scale, critical dimension scanning electron microscope (CD-SEM) tools have been and will likely continue to be one of the most commonly used metrology tools in the semiconductor industry due to their high throughput, ability to quickly examine multiple different length scales, and the relatively nondestructive nature of the measurement. This need for accurate nanometer scale measurement resolution is especially true in semiconductor lithography applications given how important line edge roughness (LER) and line width roughness (LWR) have become as performance metrics in lithography. LWR for future generations of devices is required to be $<1.5$ nm $(3\sigma)$.[1] This means that the metrology used to determine LWR must be accurate to some fraction of this length scale if the performance metric and the measurements made of it are to be meaningful.

Unfortunately, CD-SEM tools provide a two-dimensional representation of a three-dimensional (3D) structure, as can be seen in Fig. 1. There has been a significant amount of work in the photoresist community attempting to better quantify LER and to provide complete mathematical descriptors for LER, but most of this work has been based on two-dimensional line edge profiles extracted from CD-SEM data despite the fact that the majority of users do not know how accurately the SEM represents the actual roughness of the true 3D resist structure, how variations in other factors and properties (e.g., of the resist and substrate) affect these measurements, or even how the SEM actually generates the image they are analyzing in some cases. Likewise, there has been a great deal of effort in the metrology community to create better SEM simulators and to connect the experimental SEM results to three-dimensional resist feature properties such as height, width, and sidewall tilt.[2] However, most of these studies consider only perfectly smooth sidewalls, despite the fact that the roughness of these sidewalls (i.e., LER) is one of the most important problems in the semiconductor industry. To our knowledge, there has been only one other SEM simulation that explicitly considers the roughness of resist sidewalls to calculate LER, and it only considered silicon features and not organic resist patterns.[3] To address this issue, we have recently developed a detailed SEM simulation tool to examine the relationship between CD and LER as determined from SEM and true three-dimensional resist feature CD and roughness. In this article, this new SEM simulation tool is used to provide guidance on the ways in which typical SEM data and its interpretation bias the measured line width and line edge roughness of photoresist features.

[a)]Author to whom correspondence should be addressed; electronic mail: cliff.henderson@chbe.gatech.edu



Downloaded 22 Apr 2013 to 130.207.50.120. Redistribution subject to AVS license or copyright; see http://avspublications.org/jvstb/about/rights_and_permissions

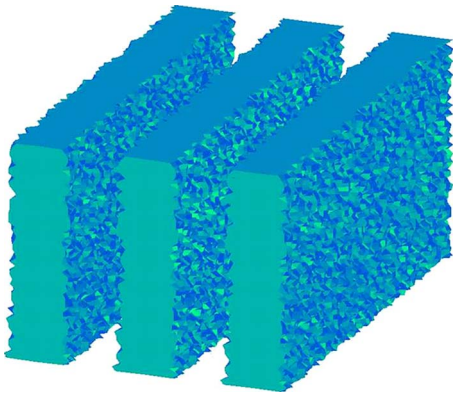

FIG. 1. (Color online) Three-dimensional representation of a resist structure. SEM converts these three-dimensional structures into a two-dimensional image.

## II. MODEL DESCRIPTION

In this work, elastic scattering is described using the differential Mott cross section for each element in the simulation. While a number of simulators use the Rutherford model and, more recently, empirical forms of the Mott cross section,[4] the full differential Mott cross section is more accurate, especially for low energy electrons. This accuracy for low energy electrons is found to be particularly important for SEM metrology and imaging applications in this work. Fortunately, the differential Mott cross section for all elements on the periodic table has been previously computed by Czyzewski *et al.*[5] and is available online.[6] The total cross section and the polar angle of the collision are determined in a similar way as described by Drouin *et al.*[7] The total elastic cross section ($\sigma_E$) is calculated by numerical integration of the differential Mott cross section as shown in Eq. (1),

$$\sigma_E = 2\pi \int_0^{\pi} \frac{d\sigma}{d\Omega} \sin\,\theta d\theta. \tag{1}$$

Likewise, the polar angle ($\theta$) of the elastic collision is calculated by Eq. (2) using a random number $R$,

$$R = \frac{\int_0^{\theta} \frac{d\sigma}{d\Omega} \sin\,\theta d\theta}{\int_0^{\pi} \frac{d\sigma}{d\Omega} \sin\,\theta d\theta}. \tag{2}$$

The elastic inverse mean free path ($\lambda_E^{-1}$) is obtained from the cross section by Eq. (3). For composite materials such as polymers, the atomic concentrations in the solid must be accounted for when calculating $\lambda_E^{-1}$ as described elsewhere,[8]

$$\lambda_E^{-1} = \frac{N_A \rho}{A} \sigma_E. \tag{3}$$

Since secondary electron emission from a sample is the primary form of information in a SEM, it is important that a model has accurate secondary generation and inelastic scattering. While the continuous slowing down approximation (CSDA) has been used widely, it does not directly provide information regarding the energy of the generated secondary electron or the characteristic energy loss due to a specific sample. Hybrid models combining the CSDA with the Moller and Vriens cross sections have also been used,[9] but it is preferred to have a unified treatment of inelastic scattering and secondary electron generation.[10] The dielectric function $\varepsilon(q,\omega)$ of a material describes its response to a given energy transfer $\omega$ and momentum transfer $q$.[11] The variable $q$ has units of inverse length and describes the momentum transfer of one particle when it collides with another particle. The dielectric function provides a unified treatment of inelastic scattering since it includes all forms of inelastic scattering from inner shell ionization to plasmon excitation. The inelastic differential cross section using the dielectric function is given by Eq. (4),[10] where $a_0$ is the Bohr radius, $\hbar\omega$ is the energy loss, $\hbar q$ is the momentum transfer, and $E$ is the energy of the electron scattering through the sample of dielectric function $\varepsilon(q,\omega)$. It is important to note that the inelastic inverse mean free path ($\lambda_I^{-1}$) given by Eq. (4) has the same units as compared to the elastic cross section ($\lambda_E^{-1}$) shown in Eq. (3),

$$\frac{d^2\lambda_I^{-1}}{d(\hbar\omega)dq} = \frac{1}{\pi a_0 E} \mathrm{Im}\left\{\frac{-1}{\varepsilon(q,\omega)}\right\}\frac{1}{q}. \tag{4}$$

While Eq. (4) would appear to provide a straightforward method for calculating inelastic cross section, $\varepsilon(q,\omega)$ is unknown for most materials. Fortunately, optical data provide $\varepsilon(0,\omega)$, i.e., $\varepsilon$ in the limit of $q=0$, and optical data are widely available for multiple different materials and compounds over a wide range of energies.[12] Penn proposed a method that has been widely used to extrapolate $\varepsilon(0,\omega)$ into the finite $q$ domain $\varepsilon(q,\omega)$.[13] This method is implemented in the model used in this work using the single-pole approximation as described by Ding and Shimizu[10] to give Eq. (5), where $\Theta$ is the Heaviside step function; given $\Theta(n)$, if $n<0$, then $\Theta(n)=0$ and if $n\geq 0$, then $\Theta(n)=1$,

$$\frac{d\lambda_I^{-1}}{d(\Delta E)} = \frac{1}{2\pi a_0 E \Delta E} \int_0^{\infty} \frac{\hbar\omega_p}{\Delta E - \hbar\omega_p} \mathrm{Im}\left\{\frac{-1}{\varepsilon(\omega_p)}\right\} d(\hbar\omega_p)\Theta \times \left[\frac{\hbar^2}{2m}(2k\bar{q} - \bar{q}^2) - \Delta E\right]. \tag{5}$$

Equation (5) is integrated as shown in Eq. (6) to give the inverse inelastic mean free path. The upper limits on the integration in Eq. (6) are chosen to be $E$ for insulators such as poly(methyl methacrylate) or PMMA as it is commonly known, but must be $E-E_F$ for semiconductors and metals, where $E_F$ is the Fermi energy of the material,

$$\lambda_I^{-1} = \int_0^{E} \frac{d\lambda_I^{-1}}{d(\Delta E)} d(\Delta E). \tag{6}$$

Likewise, the energy loss of the primary electron during an inelastic scattering event is determined by Eq. (7) using a random number $R$,



Downloaded 22 Apr 2013 to 130.207.50.120. Redistribution subject to AVS license or copyright; see http://avspublications.org/jvstb/about/rights_and_permissions

$$R = \frac{\int_0^{\Delta E} \frac{d\lambda_I^{-1}}{d(\Delta E')} d(\Delta E')}{\int_0^{E} \frac{d\lambda_I^{-1}}{d(\Delta E')} d(\Delta E')}. \quad (7)$$

The polar scattering angle for inelastic collisions is given by Eq. (8),

$$\sin\theta = \sqrt{\frac{\Delta E}{E}}. \quad (8)$$

For both elastic and inelastic scatterings, the azimuthal scattering angle is assumed to be isotropic and is given by Eq. (9),

$$\phi = 2\pi R. \quad (9)$$

Once the elastic and inelastic mean free paths have been calculated, the total mean free path of the electron can be determined using Eq. (10),

$$\lambda_T^{-1} = \lambda_E^{-1} + \lambda_I^{-1}. \quad (10)$$

A scattering event will occur when the electron has traveled a distance $s$ given by Eq. (11),

$$s = -\lambda_T \ln R. \quad (11)$$

A random number $R$ is generated and the event is considered an elastic scattering event if Eq. (12) is true; otherwise, it is considered an inelastic scattering event,

$$R < \frac{\lambda_E^{-1}}{\lambda_T^{-1}}. \quad (12)$$

Rather than recalculating inverse mean free paths, elastic polar angle, and inelastic energy loss for each iteration of a scattering event, they are calculated and tabulated as a function of energy for inverse mean free paths and as a function energy and random number for elastic polar angle and inelastic energy loss. The program interpolates these tables to determine cross sections and scattering angles. In this way, instead of having to integrate until the conditions in Eqs. (2) and (7) are met for a given random number, a random number is generated and a look-up function executed on the table determines what angle or energy loss will satisfy that condition.

The energy of the generated secondary electron is determined as described by Ding and Shimizu.[10] The binding energy of each atomic shell in a material is tabulated.[14] If the binding energy of a shell in the material is less than the energy loss of the electron, it is assumed to be an ionization scattering event and the energy of the generated secondary electron is $E_{\text{sec}}=\Delta E-E_B$. If the energy loss is less than all binding energies, then it is assumed to be a valence electron excitation and the energy of the secondary electron is $E_{\text{sec}}=\Delta E+E_F$. The polar $(\theta')$ and azimuthal scattering angles $(\phi')$ of the secondary electron are determined by Eqs. (13) and (14) using the polar and azimuthal scattering angles of the primary electron,

$$\sin\theta' = \cos\theta, \quad (13)$$

$$\phi' = \pi + \phi. \quad (14)$$

All secondary electron locations, trajectories, and energies are stored. After the primary electron energy is dissipated, all secondary electrons are sequentially called and treated the same way. This cascade process continues until all electrons have either left the sample to the detector or come to rest in the sample by dropping below a specified cutoff energy. In the case of PMMA, which is used as the resist material simulated in this work, the cutoff energy is chosen as 10 eV since the inelastic mean free path approaches infinity at energies lower than this. All electrons that scatter to a $z$ position above the top of the resist feature with an energy of 50 eV or lower are considered secondary electrons that are counted by the detector to generate the SEM signal. The materials used in this model are an organic resist consisting of pure PMMA coated onto a substrate of pure silicon. The optical constants used to calculate the inelastic mean free path for PMMA from 1 to 33 eV were obtained from the work of Ritsko *et al.*[15] The optical constants for silicon from 1 to 2000 eV were obtained from Palik.[12] Optical properties for all higher energies in both materials were obtained from the work of Henke *et al.*[16,17]

While the scattering physics used in this model are well known in the literature, the unique feature of this specific model is how it treats electron scatter on a rough resist edge. Any arbitrary structure can be generated and the only requirement is that it must be defined on a three-dimensional grid with a 1 nm lattice spacing in the case of the current model. The resist location, i.e., the lattice discretized resist feature, is fed into the model by a single file that lists the $x$, $y$, and $z$ coordinates of lattice sites that contain the resist material. In order to handle the unknown resist geometry, the electron cannot simply be advanced the full length of the scatter distance $s$ because it could pass continuously in and out of the resist material during this path length for arbitrary resist profiles, especially in the case of rough resist sidewalls. Likewise, if much of the travel distance is outside of the resist, then the next scatter event could be calculated to occur in vacuum. Instead, the scatter distance is determined for all materials present in the system, and then the travel of the electron is advanced 1 Å at a time. The scatter event occurs when the total travel distance is greater than or equal to the calculated scatter distance $s$. The travel in and out of the resist and from substrate to resist and vice versa is handled by tracking the total travel through each medium relative to the calculated $s$. When the sum of each of the fractional travel distances is equal to 1, the electron scatters in the medium in which it is currently. For example, let $s_{\text{resist}}=8$ nm and $s_{\text{substrate}}=4$ nm. If the electron travels through 6 nm of resist, it will scatter when it has traveled through 1 nm of substrate because the total travel is $\frac{3}{4}$ of $s_{\text{resist}}$ and $\frac{1}{4}$ of $s_{\text{substrate}}$. The scatter length in vacuum is considered infinity, so any travel through vacuum does not contribute to the travel distance of the electron. In this way, any arbitrary geometry or compositional nonuniformity can be handled by the model.



Downloaded 22 Apr 2013 to 130.207.50.120. Redistribution subject to AVS license or copyright; see http://avspublications.org/jvstb/about/rights_and_permissions

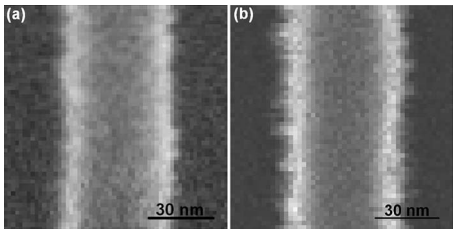


FIG. 2. Comparison of (a) SEM image measured experimentally to (b) SEM image generated by the model. The 3D line that is the source of the model SEM was generated using a mesoscale resist model set to produce a feature that is nominally identical to the experimentally patterned resist.

## III. RESULTS AND DISCUSSION

Due to the complexities of electron scatter from a patterned feature, it is very difficult to directly validate a SEM simulator with experimental SEM scans since the experimental line scans are a result of a combination of material and topographical contrast.[18] Nanoscale roughness of photoresist features makes this an even more complicated, if not impossible, task. Despite the problem with quantitative validation, the SEM simulator can be qualitatively compared with experimental SEM images to confirm that the simulator produces results that are consistent with experimental SEM scans.

Output from the SEM simulator built in this work is compared to experimental SEM data in Fig. 2 for a 100 nm long section of 50 nm thickness. The experimental SEM [Fig. 2(a)] was obtained from a negative tone molecular resist[19] sample on silicon patterned using extreme ultraviolet lithography at the Paul Scherrer Institute. The SEM was acquired using a Carl Zeiss Ultra60 SEM with a 3 keV acceleration voltage and a pixel size of 1.72 nm. The simulated SEM [Fig. 2(b)] is the simulation of a three-dimensional resist feature on silicon generated using a mesoscale resist model.[20] Figure 1 shows the kind of three-dimensional resist structure that is a typical output for the mesoscale model. The mesoscale model resist profile was generated using exposure and processing conditions, e.g., aerial image, dose, and diffusion coefficient of photoacids, estimated to be very similar to the experimental patterning conditions. PMMA was used as the material model for the SEM simulator because its dielectric properties are well known. As can be seen in Fig. 2, the SEM simulator produces results that are similar to the experimental scans. They both show similar contrast between the silicon background, edge of the line, and middle of the line. The width of the edge bloom appears to be similar in both cases as well. The simulated SEM appears to be less noisy in the bulk resist feature and substrate, but this could likely be better matched by reducing the total number of incident electrons in the simulator. The other difference between the two is that the simulation appears to have a slightly higher frequency roughness along the line edge. Overall though, the model SEM appears very similar to the experimental SEM.

While comparing the SEM images provides an overall comparison of the model to the experiment, comparing SEM line scans provides a slightly more quantitative comparison. While one would not expect to be able to directly match the SEM line scans due to differences in the roughness of each individual slice through the model, it should be able to match most of the pertinent features. Line scans from the simulation and the experimental SEM are shown in Fig. 3. To compare the experimental SEM with the model, a single line scan through four different resist lines was taken from the experimental SEM scan data described above. Rather than simulating an array of four lines in the SEM model, four different line scans were taken from different parts of the simulated resist line SEM image in Fig. 2. As expected, the line scans show similar results as in the SEM images. The contrast between substrate, bulk, and line edge are similar, and the brightness and width of the edge bloom are very similar between the model and experiment. The only obvious difference between the experimental and simulated line scans is that the substrate signal is slightly noisier in the experimental SEM data.

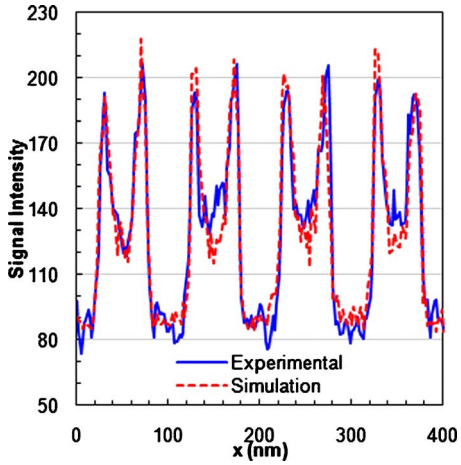


FIG. 3. (Color online) Comparison of experimentally measured line scans to typical line scans generated by the SEM simulation.

Since the SEM model reproduces experimental SEM features, it was applied to determine the difference between the SEM measured line width, i.e., the CD of the line, and the true width of the three-dimensional resist feature used to generate the SEM data. Likewise, the SEM measured line edge roughness of the line was compared to the three-dimensional sidewall roughness of the feature used to generate the SEM data. Although there are multiple different methods to define a line edge from a SEM,[21] this article uses a threshold method because it is among the most straightforward and commonly used methods in the resist literature.[22] In the threshold method, the $x$ position of the line edge is defined for each line scan in the SEM at the point where the signal intensity is greater than a specified threshold value. As the threshold is changed, the line edge position moves for a given SEM image, and thus, the measured CD and LER are influenced by this choice of threshold. This is demonstrated in Fig. 4 for three different thresholds applied to the same SEM image data. The top part of the figure shows where the line edge is defined along the resist line for the different



Downloaded 22 Apr 2013 to 130.207.50.120. Redistribution subject to AVS license or copyright; see http://avspublications.org/jvstb/about/rights_and_permissions

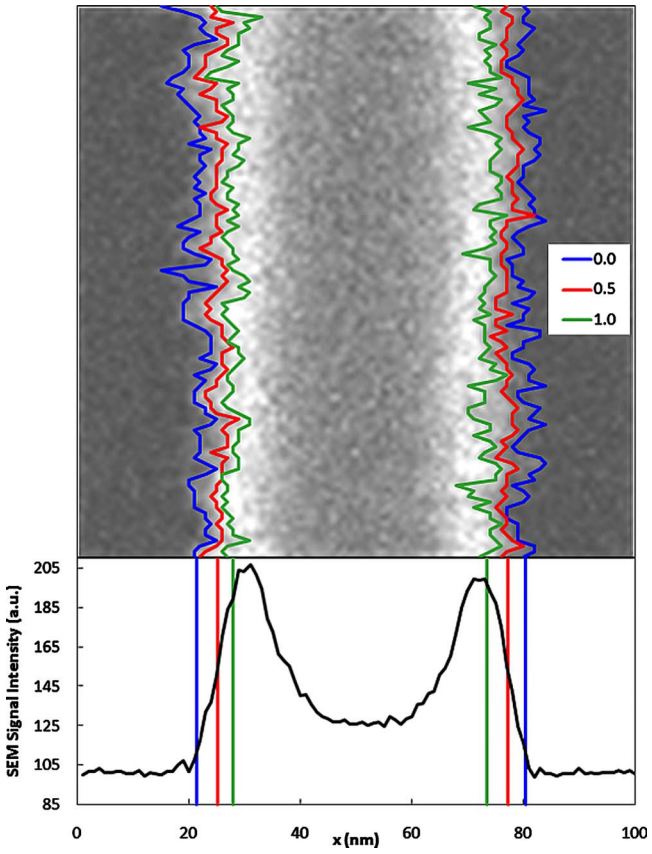


FIG. 4. (Color online) Example of how a threshold method is used to determine the line edge by displaying the line edge defined for a normalized threshold of 0, 0.5, and 1. The average line scan of the SEM is shown below to demonstrate how changing the threshold results in a shift in edge position.

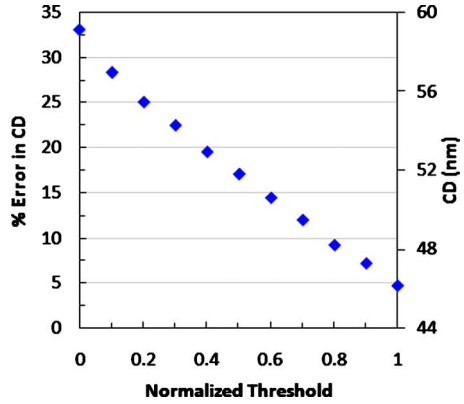


FIG. 5. (Color online) Error in SEM measured CD relative to the three-dimensional feature width as the threshold used to define the line edge is changed. The value of CD is shown on the right vertical axis to demonstrate its sensitivity to the threshold definition.

threshold values in the top-down image. The bottom part of the figure shows the average line scan profile for the resist feature along with the average edge position of the line for each of the three different threshold values. This article uses a normalized threshold that goes from the minimum threshold that is just larger than all substrate noise to the maximum threshold that defines a line entirely along a single side. As can be seen on the right side of the line scan, if a larger threshold were used, the edge definition would actually cross over to the other edge bloom before a value greater than the threshold would be encountered.

The "true" three-dimensional feature width for the resist line was determined using the rough sidewall, as can be seen in Fig. 1. Consider a single resist sidewall that runs parallel to the $y$-$z$ plane; $y$ is down the line, while $z$ is the vertical height of the line. For each lattice location in the $y$-$z$ plane, there is an $x$ position that corresponds to the outermost resist material at that $y$, $z$ coordinate. By using all of these outermost positions, the average position of the entire sidewall can be determined, and this is used to calculate the true three-dimensional feature width. The width of the resist feature analyzed in this article based on this definition of true feature size was 44.2 nm. The resulting errors in the SEM determination of CD based on this resist feature are shown in Fig. 5. The calculated CD from the SEM data can also be determined from Fig. 5 by using the right vertical axis. In all cases, the CD as determined by SEM was larger than the actual width of the resist feature.

The reason that the SEM overpredicts CD is that the average position of each resist edge is inside the rough outer peaks of the sidewall, but the SEM tends to be the most sensitive at places of highly varied topology, i.e., the rough outer peaks. If the SEM signal were proportional to the amount of material at the beam spot, then the 50% threshold would approximately be the average edge position. As the electron beam scans from the substrate into the middle of the resist feature, the signal does not increase proportionally to the amount of material it is scanning, but instead increases much more rapidly even for a relatively small amount of material. This is because it is more likely that any secondary electrons that are generated in this material will escape the resist and return to the detector than when there is a large amount of material to interact with such as in the middle of the feature, which although it generates more secondary electrons, those secondary electrons must travel a large distance to escape the resist. The SEM signal reaches a maximum at a location where there is a larger amount of material to interact, but the distance the secondary electrons have to travel to escape the resist is short. This is consistent with where the average edge location in a rough sidewall would be. As a result, when the threshold is set near the maximum, the edge defined from that threshold is closer to the actual edge position.

Figure 5 also shows that the actual calculated value of CD is strongly dependent on the choice of threshold. A significant amount of time and money is spent optimizing resist formulations and processing conditions to obtain the best performance. Many of the performance metrics are measuring using a CD-SEM. This figure shows the importance in carefully matching threshold or line definition functions when comparing two different features to ensure that only resist changes are observed, not merely changes in SEM bias.



Downloaded 22 Apr 2013 to 130.207.50.120. Redistribution subject to AVS license or copyright; see http://avspublications.org/jvstb/about/rights_and_permissions

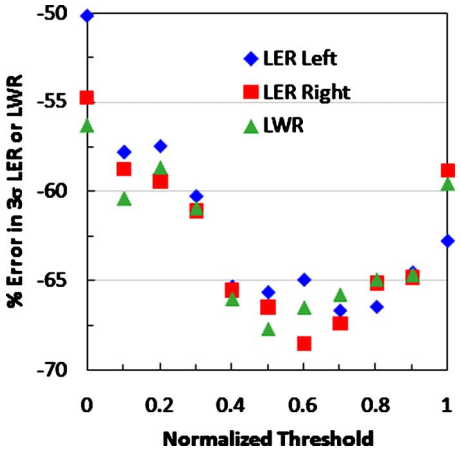


FIG. 6. (Color online) Error in SEM measured $3\sigma$ LER and LWR relative to the three-dimensional $3\sigma$ rms sidewall roughness as the threshold used to define the line edge is changed.

To compare the SEM determined LER to the actual roughness of the resist feature, the root-mean-square (rms) roughness of the sidewall is used. This rms roughness should be equivalent to the sidewall roughness that would be measured using a tilted feature with an atomic force microscope with an ultrasharp tip. The resist simulated in Fig. 4 has a left sidewall rms roughness ($1\sigma$) of 4.19 nm and a right sidewall roughness ($1\sigma$) of 3.95 nm; this is consistent with the experimentally measured resist sidewall roughness of 4.5 nm by Goldfarb *et al.*[23] The error in the SEM measured LER for each side relative to the sidewall roughness is shown in Fig. 6. The error increases at middle thresholds relative to lower and higher thresholds simply because the SEM line scans at these thresholds tend to be less noisy, as can be seen in Fig. 4, which tends to cause a lower calculated LER.

The SEM measured LER tends to significantly underpredict the true rms roughness of the feature, regardless of the threshold used. The right LER ($3\sigma$) goes from 5.36 to 3.96 nm at thresholds of 0 and 0.5, respectively, and back up to a value of 4.88 nm at a threshold of 1; this is compared to the rms sidewall roughness ($3\sigma$) of 11.9 nm. The error in the LER measured by SEM is so large that the $3\sigma$ LER is almost the same as the $1\sigma$ rms roughness. This is a large underprediction of true sidewall roughness, but is consistent with the results of Li *et al.*,[3] which show approximately 50% error in LER relative to sidewall roughness for silicon lines. Several other resist features were generated, and the LER for those features as determined from the simulator still tends to be lower than the true sidewall roughness.

It is currently unknown what effect the amplitude of the resist sidewall roughness has on device performance. Nearly all studies examining the effect of roughness on device performance use LER and LWR determined from SEM as the primary metric for roughness. Using LWR as a metric, it has been determined that LWR needs to remain below 8% of the CD to maintain device reliability and performance.[1] Since these studies used LER as the metric, it is conceivable that this 8% implicitly includes the fact that the sidewall roughness is actually greater than 8% of CD and the devices still perform well. However, as $3\sigma$ LWR must shrink below 2 nm for future generations of devices, the 8% rule may no longer be sufficient since the sidewall roughness is much greater than expected.

## IV. CONCLUSIONS

A rigorous Monte Carlo simulation of scanning electron microscopy has been developed to probe the relationship between the roughness of a three-dimensional resist feature and the line edge roughness as measured by SEM. The model appears to accurately reproduce both the full image and individual line scans of resist features from an experimental SEM. The critical dimension of the resist determined from SEM best matches the true resist feature width when the line edge is defined using a high threshold because the roughness on the outer edge of the resist tends to cause an increase in SEM signal that is nonproportional to the amount of material on the outer edge of the feature. It was found that LER determined from the SEM is significantly smaller than the true resist feature sidewall roughness. The measured LER is typically more than 50% smaller than the actual sidewall roughness.

## ACKNOWLEDGMENT

The authors gratefully acknowledge Intel Corporation for funding this research.

[1]See http://www.itrs.net/
[2]J. S. Villarrubia and Z. J. Ding, J. Micro/Nanolith. MEMS MOEMS **8**, 033003 (2009).
[3]Y. G. Li, S. F. Mao, H. M. Li, S. M. Xiao, and Z. J. Ding, J. Appl. Phys. **104**, 064901 (2008).
[4]R. Browning, T. Z. Li, B. Chui, J. Ye, R. F. W. Pease, Z. Czyzewski, and D. C. Joy, J. Appl. Phys. **76**, 2016 (1994).
[5]Z. Czyżewski, D. O. MacCallum, A. Romig, and D. C. Joy, J. Appl. Phys. **68**, 3066 (1990).
[6]See http://web.utk.edu/~srcutk/
[7]D. Drouin, P. Hovington, and R. Gauvin, Scanning **19**, 20 (1997).
[8]P. Hovington, D. Drouin, and R. Gauvin, Scanning **19**, 1 (1997).
[9]B. Wu and A. R. Neureuther, J. Vac. Sci. Technol. B **19**, 2508 (2001).
[10]Z. J. Ding and R. Shimizu, Scanning **18**, 92 (1996).
[11]J. C. Ashley, J. Electron Spectrosc. Relat. Phenom. **50**, 323 (1990).
[12]E. D. Palik, *Handbook of Optical Constants of Soilds, Vol 1* (Academic, New York, 1985), Vol. 1, pp. 547–569.
[13]D. R. Penn, Phys. Rev. B **35**, 482 (1987).
[14]See http://xdb.lbl.gov/Section1/Sec_1-1.html
[15]J. J. Ritsko, L. J. Brillson, R. W. Bigelow, and T. J. Fabish, J. Chem. Phys. **69**, 3931 (1978).
[16]See http://henke.lbl.gov/optical_constants/
[17]B. L. Henke, E. M. Gullikson, and J. C. Davis, At. Data Nucl. Data Tables **54**, 181 (1993).
[18]M. Dapor, M. Ciappa, and W. Fichtner, J. Micro/Nanolith. MEMS MOEMS **9**, 023001 (2010).
[19]R. A. Lawson, L. M. Tolbert, T. R. Younkin, and C. L. Henderson, Proc. SPIE **7273**, 72733E (2009).
[20]R. A. Lawson and C. L. Henderson, Proc. SPIE **7639**, 76392G (2010).
[21]J. S. Villarrubia, A. E. Vladár, and M. T. Postek, J. Microlithogr., Microfabr., Microsyst. **4**, 033002 (2005).
[22]C. N. Anderson and P. P. Naulleau, J. Vac. Sci. Technol. B **27**, 6 (2009).
[23]D. L. Goldfarb *et al.*, J. Vac. Sci. Technol. B **22**, 647 (2004).



Downloaded 22 Apr 2013 to 130.207.50.120. Redistribution subject to AVS license or copyright; see http://avspublications.org/jvstb/about/rights_and_permissions